geosciences

MDPI

Article

Geochemical Characteristics of the Volcanic Rocks Associated with Boron-Rich Deposits from the Xiongba Basin, Qinghai–Tibet Plateau

Wenxi Chen, Xifang Liu, Yuanyi Zhao and Yongjie Lin *

MNR Key Laboratory of Saline Lake Resources and Environments, Institute of Mineral Resources, Chinese Academy of Geological Sciences, Beijing 100037, China; chenwenxi@mail.cgs.cn (W.C.); liuxifang369@163.com (X.L.); yuanyizhao2@sina.com (Y.Z.)
* Correspondence: linyongjie2014@163.com

Abstract: The Qinghai–Tibet Plateau (QTP) hosts significant lacustrine sedimentary boron-rich deposits, with the Xiongba Basin being a prominent region housing two large sedimentary boron-rich deposits. These deposits are closely associated with extensive Neogene volcanic rocks. This study investigates the origin and boron sources of Miocene volcanic rocks in the Xiangqu River area, located within the Xiongba Basin. The volcanic rocks in the basin comprise ultrapotassic andesites, ultrapotassic trachyte, potassic trachyte, and potassic trachyandeiste. The trace element content and the active/inert elements ratios of the studied volcanic rocks have indicated that they were generated in a subduction environment and were influenced by enrichment fluids derived from deep-sea sediments or altered oceanic crust during their formation. Accordingly, the studied volcanic rocks exhibit significant boron enrichment. The eruption of magma and subsequent hydrothermal activity released boron, which became the primary source for the lacustrine sedimentary boron-rich deposits within the basin. The arc-like trace element features (e.g., Nb-Ta depletion relative to La and K) and high B concentrations in these rocks were inherited from the mantle source, which had been enriched by melt/fluid of the subducted sediments. A two-stage evolutionary model is proposed to explain the enrichment of B in subduction environments, as well as the subsequent melting of the B-enriched source during a post-collisional setting. These findings highlight the potential for boron and lithium mineralization in similar volcanic rock-bearing regions across the QTP. Future exploration efforts in such areas could provide valuable insights into the formation processes of lacustrine sedimentary boron-rich deposits and contribute to the understanding of boron and lithium resource potential.

Keywords: Xiongba Basin; Neogene; volcanic rocks; geochemical characteristics; boron source

check for updates

Citation: Chen, W.; Liu, X.; Zhao, Y.; Lin, Y. Geochemical Characteristics of the Volcanic Rocks Associated with Boron-Rich Deposits from the Xiongba Basin, Qinghai–Tibet Plateau. *Geosciences* **2023**, *13*, 265. https://doi.org/10.3390/geosciences13090265

Academic Editors: Feng Guo and Jesus Martinez-Frias

Received: 16 June 2023
Revised: 19 August 2023
Accepted: 21 August 2023
Published: 31 August 2023

Copyright: © 2023 by the authors. Licensee MDPI, Basel, Switzerland. This article is an open access article distributed under the terms and conditions of the Creative Commons Attribution (CC BY) license (https://creativecommons.org/licenses/by/4.0/).

1. Introduction

Lacustrine sedimentary boron-rich deposits are of great industrial significance and large in scale among the various types of boron deposits known worldwide [1–3]. The occurrence of significant borate deposits worldwide is consistently associated with endorheic basins situated in active volcanic regions that are subject to extensional tectonic regimes, where hydrothermal or geothermal waters facilitate the leaching of boron from the surrounding volcanic rocks and serve as a conduit for its transportation into temporary alkaline lakes [2–5]. Borate minerals (borax, ulexite, colemanite, etc.) are the major source of commercial boron (B) and are largely concentrated in lacustrine deposits within two main mineralization zones: the North–South Cordillera–Andes zone and the East–West Alps–Himalayas zone [1–3,6]. Lacustrine borate deposits are consistently found in close geological proximity to Miocene volcanogenic rocks, in addition to being limited to a specific range of environmental and tectonic conditions [7].

The borate deposits of the Qinghai–Tibet Plateau (QTP) within the eastern Alps–Himalayas zone are closely associated in space and time with Miocene tuffs and lavas [6]. The collision between the Indian and the Eurasian Plates resulted in significant uplift of the QTP and extensive Miocene volcanic activity in its interior, making it an important source of these boron deposits [8,9]. The Xiongba Basin in QTP is characterized by the widespread occurrence of lacustrine volcanic–sedimentary boron deposits that are associated with large-scale Miocene volcanic rocks [6,10,11]. The source of B in this area is thus often linked to form through the leaching of volcanic rock by geothermal water and atmospheric precipitation. The B was carried by the Xiongqu River into the lake basin and eventually formed through borate minerals precipitation resulting from arid events since the Quaternary period [12].

This study focuses on investigating the geochemical characteristics of Miocene intermediate volcanic rocks associated with lacustrine boron-rich deposits in the QTP, specifically targeting the Nieèr Co and Chagcam Caka borate deposits. Through comprehensive analysis of whole-rock geochemical data encompassing major, trace, and rare earth elements, our research aims to enhance our understanding of the petrogenesis of these volcanic rocks. Additionally, we aim to unravel the processes of crustal melting and assimilation within silicic volcanic rocks, shedding light on their association with B-rich ore-forming systems. The significance of this study lies in its potential to contribute to a deeper comprehension of the geological and geochemical processes that have shaped the Xiongba Basin and facilitated the formation of borate deposits within it. Moreover, the findings hold broader implications for analogous geological settings worldwide. By expanding our knowledge of the formation mechanisms of lacustrine borate deposits and their relationship with silicic volcanic rocks, this research contributes to the broader understanding of borate mineralization in various geological contexts.

2. Geological Setting

The QTP comprises four distinct blocks: the Songpan–Ganzi block, Qiangtang block, Lhasa block, and Himalayan block, which are separated by three suture zones: the Jinsha River suture zone (JSSZ), Bangong–Nujiang suture zone (BNSZ), and India–Yarlung Zangbo suture zone (IYZSZ) [13,14] (Figure 1). The Lhasa block is further subdivided into three secondary blocks, namely, the northern, central, and southern blocks, by the Shiquan River–Nam Co ophiolite belt (SNMZ) and the Lhoba–Dianzhong fault (LMF) [15]. The study area is located in the western part of the Lhasa block in the Xiongba Basin. The Nieer Lake fault zone is situated to the north of the basin, while the Bangba fault zone is located to the south. The study area displays well-developed linear structures, and the main tectonic lines trend in an east–west direction, reflecting the effects of the principal compressive stress field from the north and south. The Xiongba Basin contains multicolored coarse clastic sedimentary strata of the Paleogene Niubao Formation, composed mainly of clastic rocks, including unmetamorphosed sandstones, sandstones, and conglomerates, and volcanic rocks of the Paleogene Linzizong Group are found in the southern and southeastern parts of the basin [12]. In the southeastern part of the basin, there are unconformable contacts between Permian–Jurassic metamorphic sandstones, sandstones, and slate and the Linzizong Group. The Cretaceous–Paleogene granitic intrusion is widespread in the basin, intruding into the sedimentary and metamorphic sedimentary strata of the Permian to Jurassic period. The primary stratum in the basin is the Neogene Xiongba Formation, which is a volcanic–sedimentary formation with lacustrine facies. In the northern part of the basin, relatively intact volcanic craters can be found.

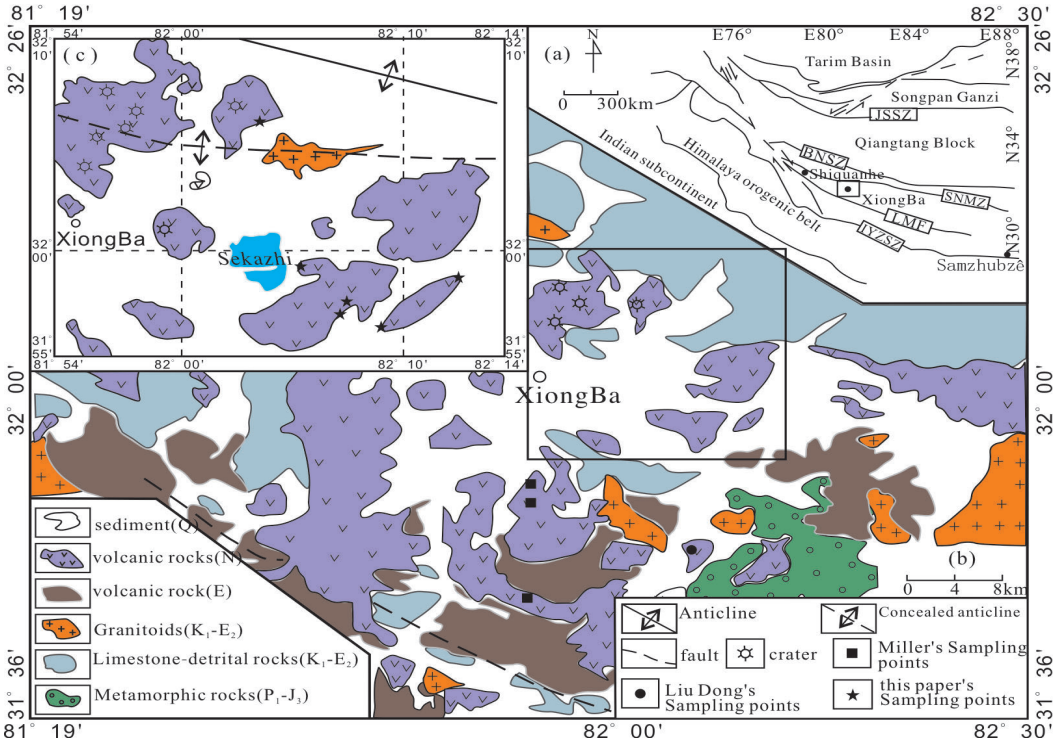

Figure 1. (**a**) Simplified geological map of the tectonic outline in the southwestern Tibetan Plateau; (**b**) simplified geological map of Xiongba volcanic rock; (**c**) distribution diagram of volcanic rocks that are volcanic–sedimentary in the Xiongba Basin [16]. JSSZ—Jinshajiang Suture Zone; BNSZ—Bangong–Nujiang Suture Zone; SNMZ—Shiquan River–Nam Tso Ophiolitic Melange Zone; LMF—Luobadui–Mila Mountain Fault; IYZSZ—Indus–Yarlung Zangbo Suture Zone; NL—Northern Lhasa block; ML—Middle Lhasa block; SL-Southern Lhasa block

3. Materials and Methods

In this study, we conducted fieldwork in the Sekdo region to collect fresh samples from the volcanic rocks of the Xiongba Formation's volcanic–sedimentary strata (see Figure 2). Stratigraphic sampling was employed, targeting well-exposed volcanic rock outcrops. Each sample collected weighed over 1 kg. Subsequently, the samples were manually crushed into small pieces, and careful selection was made to obtain fresh, almond-free mixed samples of approximately 100 g. These selected samples were then ground to a particle size of 200 mesh. The major and trace element analysis was performed at the China National Geological Experimental Testing Center using X-ray fluorescence spectrometry (PW4400) and inductively coupled plasma mass spectrometry (Agilent ICP-MS 7900). Loss on ignition (LOI) was determined by weighing the samples before and after heating them at 1075 ± 25 °C for 1 h. The detailed operating procedures and conditions for XRF and ICP-MS analysis were consistent with those described by Yang et al. [17] and Lin et al. [18], respectively. The analysis precision for major element data was better than 0.05%, and the analytical uncertainties for trace elements were better than ±5% (wt.%) and under ±1% for measuring rare earth elements (REE) for repeated analyses of Chinese national standards GB/T 14506.14-2010 and GB/T 14506.28-2010. The REE data were normalized to Post-Archean Australian Shale (PAAS) [19], and PAAS-normalized anomalies were calculated as follows [20]: $Ce/Ce^* = 2Ce_{SN}/(La_{SN} + Pr_{SN})$, $Eu/Eu^* = 3Eu_{SN}/(2Sm_{SN} + Tb_{SN})$, and $Pr/Pr^* = 2Pr_{SN}/(Ce_{SN} + Nd_{SN})$.

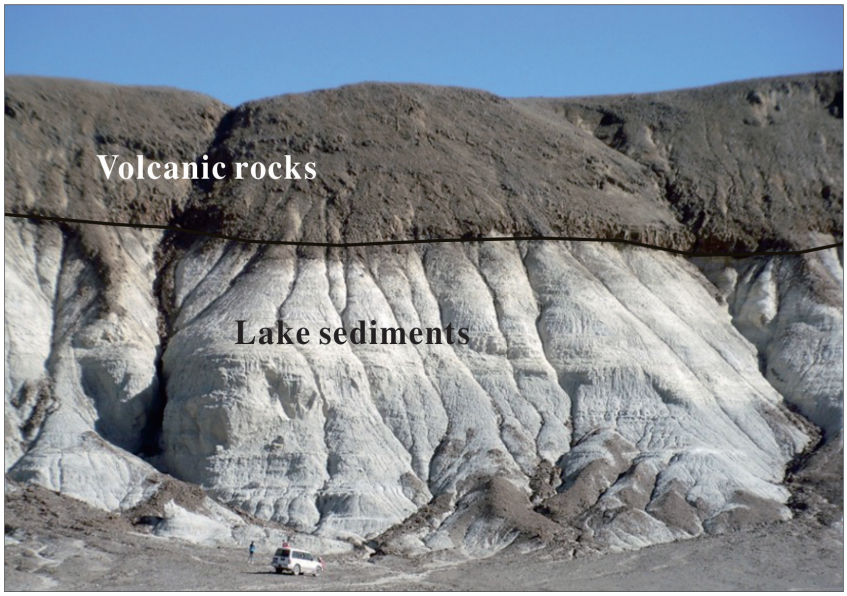

Figure 2. Volcanic sedimentary strata of the Xiongba Formation.

4. Results

4.1. Petrological Results

The Xiongba Formation volcanic rocks in this study are primarily distributed in the Sekazi area and represent the uppermost section of the volcanic rocks in the Xiongba Formation. These rocks are characterized by an overall gray or gray-black color and exhibit speckled, vesicular, and blocky structures. The dominant phenocrysts found in these volcanic rocks are black mica. The volcanic rocks in the study area primarily consist of andesite, trachyte, and trachydiorite. The andesite is characterized by a gray-black color and contains spotted and blocky structures. The primary mineral components include common pyroxene, biotite, quartz, and plagioclase. Spotted crystals, which account for 30% to 45% of the composition, mainly consist of biotite, followed by common pyroxene, plagioclase, and a small amount of quartz. These crystals have formed harbor-shaped structures due to resorption. The matrix of the andesite has a glass interweaving structure, mainly composed of plagioclase, sericite, cryptocrystalline materials, and vesicle. The trachyte is also characterized by a gray-black color with a small amount of broken and clustered spotted crystals, accounting for approximately 40% of the composition. The main mineral components are biotite, common pyroxene, glomerocryst, feldspar, clustered neutral feldspar, and occasional fractured and corroded quartz. The matrix has a glass and basic interweaving structure, with tiny plagioclase crystals dispersed in the glass. The trachydiorite has a gray-black color with spotted and interweaving structures. The spotted crystals, which account for approximately 30% of the composition, mainly consist of biotite, occasionally hornblende and quartz. The matrix has a stripe-shaped plagioclase interweaving structure that makes up about 60% to 75% of the rock. There are almond-shaped structures filled with vesicle, accounting for 10%, which are irregularly shaped, and some are filled with silica. After the silica loses its glassy nature, they are replaced by radially arranged fibers of quartz.

4.2. Major Elements

The volcanic rocks collected from the Xiongba Basin exhibit alkaline characteristics, with a total alkali content ($K_2O + Na_2O$) ranging from 7.53 wt.% to 9.7 wt.% and SiO_2 contents ranging from 56.39 wt.% to 64.85 wt.% (Table 1). The TAS diagram classifies the Neogene volcanic rocks in the Xiongba Basin as belonging to the alkaline series of trachyandesite and trachydacite. The alkaline volcanic rocks in the Xiongba Basin consist of trachydacite and trachyandesite, most of them falling within the range of potassic–

ultrapotassic volcanic rocks of the Lhasa terrane (see Figure 3a). In the SiO_2 and K_2O diagram (see Figure 3a), the volcanic rocks are classified as potassic intermediate-felsic rocks, characterized by $K_2O > Na_2O$, $K_2O + Na_2O$ ranging from 7.53 wt.% to 9.7 wt.%, $K_2O/Na_2O > 2$, and K_2O ranging from 5.17 wt.% to 7.73 wt.%. The major elements of the rock samples show Al_2O_3 concentrations ranging from 11.77% to 15.29% and MgO concentrations ranging from 2.35 wt.% to 6.39 wt.%. Specifically, the MgO values of potassic trachyandesite and potassic andesitic trachyte are less than 3 wt.%, while the MgO values of ultrapotassic andesitic trachyte are greater than 3 wt.%.

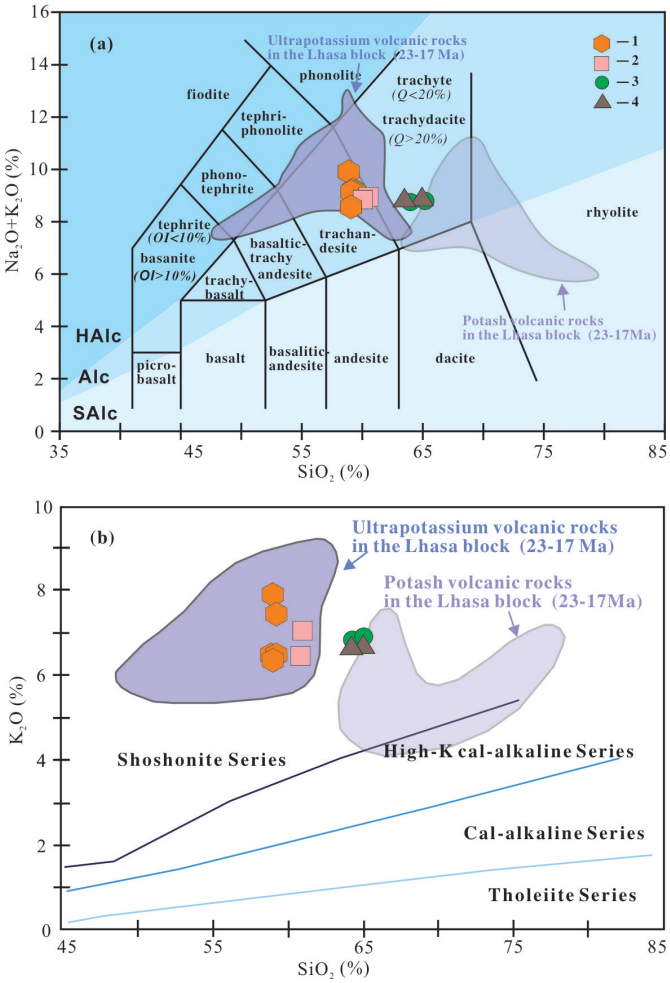

Figure 3. Total alkali-silica (TAS) diagram (after Irvine et al., 1971 [21]; Bas et al., 1986 [22]); (**b**) K_2O-SiO_2 diagram (after Rickwood et al., 1989 [23]); the potassic–ultrapotassic rocks in the Lhasa block (after Liu et al., 2011 [16]) (1—ultrapotassic andesite; 2—ultrapotassic trachyte; 3—potassic trachyandeiste; 4—potassic trachyte).

Table 1. The major element composition for the volcanic rock samples.

Sample	D2B8	D2B10	D2B11	D2B12	D8B3	D8B4	D8B7	D8B8	D8B17	D8B18	D8B19	SKP1-14	SKP1-15
SiO_2	57.96	57.71	56.39	58.1	62.48	64.21	57.27	57.78	59.26	58.62	58.13	63.26	64.85
TiO_2	1.08	1.07	1.04	1.08	0.65	0.68	1.35	1.31	1.11	1.11	1.11	1.12	1.1
Al_2O_3	12.63	12.7	12.55	12.69	14.92	15.29	12.48	12.62	13.04	13.85	12.87	11.77	11.79
Fe_2O_3	4.47	4.95	4.39	4.49	2.99	3.07	5.29	5.37	4.65	4.5	3.98	6.15	4.41
MnO	0.08	0.08	0.07	0.08	0.05	0.04	0.09	0.08	0.08	0.06	0.06	0.12	0.04
MgO	6.39	6.19	5.74	6.26	1.65	1.5	5.64	6.09	4.91	4.16	4.84	2.35	2.48
CaO	5.22	4.8	5.49	5.08	4.36	2.95	4.13	4.07	4.5	4.92	5.49	2.02	1.66
Na_2O	2.54	2.53	1.37	2.55	2.18	2.15	1.97	1.9	1.83	2.18	1.63	1.73	2.13
K_2O	6.35	6.44	6.16	6.41	6.33	6.66	7.73	7.33	6.85	6.35	6.78	6.88	6.70
P_2O_5	0.99	0.97	0.98	1.02	0.25	0.25	0.87	0.82	0.65	0.62	0.65	0.85	0.87
LOI	0.94	0.9	4.31	0.81	3.12	1.99	1.92	0.89	2.08	2.29	3.45	2.38	1.86

Based on the definition of potassic rocks, characterized by high K_2O content and $K_2O/Na_2O > 1$, as well as the definition of ultrapotassic volcanic rocks, having MgO > 3 wt.%, K_2O > 3 wt.%, and K_2O/Na_2O > 2 [7,24], and considering the rock classification chart and the range of potassic and ultrapotassic volcanic rocks in the Lhasa terrane [16], the volcanic rocks found in the Xiongba Basin can be classified into four distinct types: ultrapotassic andesite, ultrapotassic trachyte, potassic trachyte, and potassic trachyandesite.

4.3. Trace and Rare Earth Elements

The ΣREE values of the studied volcanic rocks from the Xiongba Basin range from 337 ppm to 836 ppm with an average of 579 ppm (Figure 4 and Table 2). The LREEs (light rare earth elements) and HREEs (heavy rare earth elements) average values are 553 ppm and 26 ppm, respectively. In general, the chondrite-normalized REE patterns of the volcanic rocks showed the following characteristics: (1) significant LREEs enrichment [$(La/Yb)_N$= 3.49–6.24, avg. = 4.72]; (2) no obvious Ce anomaly; (3) slight negative Eu anomalies (Eu/Eu^* = 0.51–0.63, avg. = 0.55). The LREEs/HREEs ratio ranges from 18.50 to 31.37, indicating a high degree of differentiation. Among the volcanic rocks analyzed, the potassium trachyte andesite exhibits higher ΣREE, LREE, and HREE values than the ultrapotassic andesite and the ultrapotassic trachyte, while the potassic trachyte shows the lowest values. The spider diagram of trace elements normalized to the primitive mantle indicates that the distribution patterns of trace elements in the studied volcanic rocks are similar (Figure 4b). The studied volcanic rocks are enriched in large ion lithophile elements (LILE) such as Th, K, and Pb, while high-field strength elements (HFSE) such as Nb, P, and Ti are relatively depleted, suggesting the crustal contamination in such setting [25]. Another contributing factor to these geochemical characteristics might be the processes of apatite and Fe-Ti oxide fractionation.

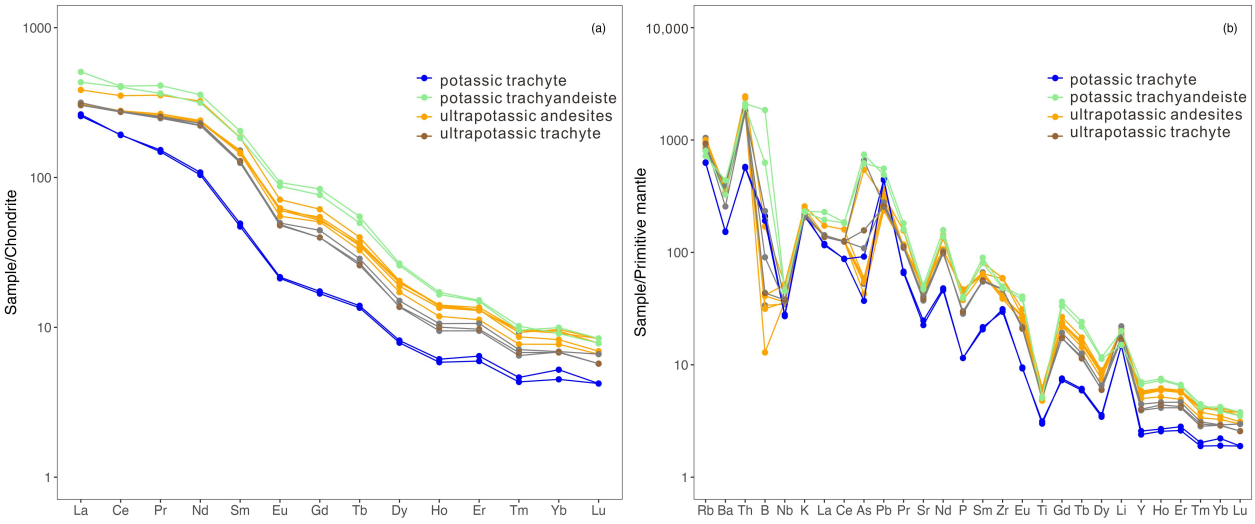

Figure 4. Rare earth elements (REE) (**a**) and trace elements (**b**) abundances of volcanic rocks from the Xiongba Basin normalized to chondrite [26] and primitive mantle [27], respectively.

Table 2. The trace and rare earth element composition for the volcanic rock samples.

Sample	D2B8	D2B10	D2B11	D2B12	D8B3	D8B4	D8B7	D8B8	D8B17	D8B18	D8B19	SKP1-14	SKP1-15
Li	33	32.5	31.7	30.7	23.8	23.7	29.8	30.3	35.2	28.1	26.8	24	31.9
Be	12.9	13.6	10.4	11.5	12.9	13.6	14	12.4	10.1	9.25	10	11	11.5
Sc	14.6	15.4	13.7	15.7	-	-	-	-	12.5	12.7	12.8	13.7	11.1
V	105	109	106	99.8	57.4	58.8	87.2	103	101	98.8	97.1	101	103
Cr	385	401	374	381	45.8	47.7	424	428	279	260	283	437	469
Co	26.7	46.9	20.9	22.1	8.21	6.98	23.5	26.7	22.4	16.5	23.1	39.6	30.6
Ni	263	290	178	195	16.3	13.3	259	288	164	94.3	157	232	221
Cu	57.2	51.6	63.1	54.1	10.6	7.48	44.3	41.1	28	22.9	24.8	33.3	41.9
Zn	85.7	110	58.5	73.5	63.1	60	71.2	75.1	69.8	72.6	70.7	74.5	107
Ga	21.9	22.5	20.6	21.3	26.7	27.3	22.6	22.8	22	23.5	22	19.7	21.2
Rb	664	636	546	587	401	398	605	607	590	524	586	458	509
Sr	974	1035	1034	1071	522	476	880	822	787	854	819	994	1072
Zr	450	466	434	459	332	350	663	657	525	524	530	537	557
Nb	24.7	25.7	25.6	26	19.3	19.9	37.3	36.7	26.6	26.1	27	32.4	32.3
Ba	2551	2385	2578	2366	1073	1063	2734	2658	1791	2757	2299	3059	2283
Hf	12.6	12.6	11.8	13	-	-	-	-	15.2	14	14.5	14.8	14.8
Ta	1.45	1.45	1.46	1.59	-	-	-	-	1.46	1.48	1.55	1.77	1.69
Pb	47.6	48.7	56.9	43.8	82.7	81.4	59.2	66.9	48.7	51.5	47.3	90.9	103
Th	153	152	144	153	48.1	49	208	201	150	156	150	168	179
U	23.9	23.5	21.7	22.3	-	-	-	-	19.4	17.2	22.3	20.4	19.2
As	5.26	5.88	54.3	4.27	9.18	3.71	5.89	5.46	65.8	10.9	15.7	74.2	62.1
Mn	552	661	517	629	382	345	651	626	618	462	496	781	324
B	20.3	24.6	18.9	7.73	115	126	102	25	140	54.3	26.1	377	1109
La	95.6	96.6	97	97.2	81.7	79.6	119	97.2	94.1	97.8	94.5	134	157
Ce	223	225	222	223	155	156	284	223	221	223	222	324	329
Pr	31.6	32.4	31.7	31.3	18.6	18.1	43.2	31.3	30.3	31.1	30.9	44.4	50.1
Nd	142	144	141	141	64.8	62.4	194	141	133	138	134	189	214
Sm	29.5	28.7	28.2	28.7	9.6	9.18	36	28.7	24.4	25.1	25	35.8	39.8
Eu	4.44	4.42	4.05	4.58	1.59	1.56	5.23	4.58	3.57	3.65	3.52	6.43	6.8
Gd	13.4	14.1	13.1	13.7	4.5	4.35	15.9	13.7	10.3	11.5	10.3	19.8	21.7
Tb	1.7	1.74	1.55	1.66	0.66	0.64	1.89	1.66	1.27	1.36	1.23	2.36	2.6
Dy	6.37	6.51	5.53	6.07	2.63	2.54	6.57	6.07	4.4	4.84	4.44	8.34	8.58
Ho	1.01	1.01	0.85	0.97	0.44	0.42	0.99	0.97	0.68	0.76	0.72	1.19	1.23
Er	2.75	2.85	2.36	2.72	1.35	1.25	2.76	2.72	1.99	2.23	2.04	3.13	3.18
Tm	0.3	0.31	0.25	0.31	0.15	0.14	0.28	0.31	0.21	0.23	0.22	0.31	0.33
Yb	2.02	1.91	1.61	1.97	1.09	0.94	1.73	1.97	1.43	1.44	1.42	2.08	1.9
Lu	0.28	0.28	0.22	0.26	0.14	0.14	0.23	0.26	0.19	0.22	0.19	0.28	0.26
Y	25.9	26.6	22.8	24.7	11.7	10.9	25.4	26	17.9	20.3	18.3	30.4	31.9

4.4. Characteristics of B Content in Volcanic Rocks

The Xiongba Basin is known for its volcanic rocks of various ages, and the volcanic rocks of the Xiongba Formation are primarily found in the Sekazi region [16,28,29]. These rocks exhibit a combination of volcanic and sedimentary features, with lithological assemblages consisting of trachyte and trachydacite explosive rocks. The boron content of these rocks varies significantly (Table 2), ranging from 7.73 to 1109 ppm. The ultrapotassic andesite has the lowest boron content, while the potassium trachyte andesite has the highest. The boron content of ultrapotassic andesite ranges from 7.73 to 102 ppm, displaying a relatively large variation range with an average value of 33.09 ppm. The potash trachyte has a boron content ranging from 115 to 126 ppm, with an average of 121 ppm. The ultra potassium trachyte exhibits a boron content ranging from 26 ppm to 140 ppm. The potassium trachyte andesite, on the other hand, has the highest boron content, ranging from 337 ppm to 1109 ppm, with an average of 743 ppm. The boron content of these rocks demonstrates a strong positive correlation with their SiO_2 content. B is considered an incompatible element that tends to migrate along with Pb, Li, As, and Be in subduction environments [7]. In the studied volcanic rocks, B displays a positive correlation with Pb, Li, and Be but shows a greater variation when compared to As.

5. Discussions

5.1. Genesis of Miocene Volcanic Rocks in Xiongba Basin

The origin of ultrapotassic andesites is thought to involve partial melting of a mantle source that is highly enriched in K, leading to their elevated K content and unique geochemical characteristics [30–32]. This mantle source is believed to have undergone metasomatism, a process of alteration by fluids, which is associated with subduction or mantle plume activity. The partial melting of this enriched and modified mantle source produces magmas with high K and low Al content, which are then transported to the

surface to form ultrapotassic andesites [32,33]. The enrichment in incompatible elements is likely a result of the addition of fluids or melts from the subducting plate or mantle plume, which modify the composition of the mantle source [34]. The melting process may also involve the addition of subducted material or lithospheric mantle, which can further modify the geochemical signature of the resulting magmas [34,35]. The chemical composition of ultrapotassic andesites is characterized by LILE such as Rb, K, Pb, and LREE enrichment, while HFSE (e.g., Nb, P, and Ti) and HREE are significantly depleted [36]. The high MgO values, as well as high Cr and Ni values relative to the crustal average [37], indicate that they originate from enriched mantle sources and have characteristics of primitive magma. This is due to the involvement of continental crustal material in the Lhasa terrane mantle tectonic activity during the subduction of the Indian continental lithosphere beneath the northern margin of the Indian continent [29,38].

Potassic trachyandesites are thought to have originated from the partial melting of basaltic rocks that underwent metasomatism in the mantle wedge [24,39]. This melting produces magmas with high K and low Al content, which are then transported to the surface to form potassic andesites. In some cases, potassic andesites can also be generated by the mixing of different magma types, including melts from the mantle and crust, leading to hybrid compositions [40,41]. Potassic trachyte andesites in this study exhibit LILE and HREE enrichment, as well as HFSE and HREE depletion. The Cr and Ni contents range from 45.8 to 47.7 ppm and 13.3 to 16.3 ppm, respectively, which are similar to the crustal. They share similar characteristics with Chaga-tsé volcanic rocks and may have originated from partial melting of the enriched potassium-rich material in the lower crust of the Lhasa terrane [42].

The volcanic rock known as ultrapotassic trachyte has a unique composition with high potassium content and fine-grained texture. It forms through the partial melting of enriched mantle sources [43], often in post-collisional or within-plate settings [44]. Subduction-induced heat and pressure trigger mantle rock melting, leading to volcanic eruptions upon ascent. As the magma cools, it solidifies into various volcanic rocks, including ultrapotassic trachyte [43,45]. Ultrapotassic trachyte's origin ties to plate tectonics, driving Earth's lithosphere movement and rock formation. Average ytterbium (Yb) and yttrium (Y) concentrations in ultrapotassic trachyte stand at 1.43 ppm and 18.83 ppm, consistent with adakitic rocks from crustal melting, suggesting a lower crust origin [46]. Trachyte/syenite magmas form at pressures around 15×10^8 Pascals (equivalent to a 55 km thick crust), with plagioclase retaining negative europium (Eu) anomalies. At 17×10^8 Pascals (60 km crust), plagioclase transforms into clinopyroxene, leading to trachyandesitic/monzonitic magmas without negative Eu anomalies [47]. In the study area, ultrapotassic trachyte shows faint negative Eu anomalies and Rb/Sr ratios between 0.61 and 0.75, implying deeper magma origins [48,49]. All samples have negative Eu anomalies around 0.5, indicating plagioclase fractionation or melting depths within plagioclase stability (<30 km).

Potassic trachyte is formed through volcanic activity, which is associated with volcanic regions that are rich in alkali metals such as K and Na. In general, potash trachyte is formed when magma containing high levels of K and Na slowly cools and solidifies, either above or below the earth's surface [50]. As the magma cools, minerals such as alkali feldspar, mica, hornblende, and biotite crystallize and combine to form the characteristic fine-grained texture of trachyte. Potash trachyte can be found in various geologic environments, including volcanic fields, calderas, and rift zones. It is often associated with other volcanic rocks such as basalt, andesite, and rhyolite, and can be found in both extrusive and intrusive forms [50,51]. The potash trachyte examined in this study displays typical features including high concentrations of Mg and compatible elements such as Cr and Ni, high contents of rare earth elements (REEs) and trace elements, enrichment in LILEs and depletion in HFSEs, high Th/Ta ratios (94.91–105.92), low Nd/La ratios (0.18–0.22), and low Rb/Ba ratios (0.14–0.15). These characteristics are similar to those of Xiongba Basin potassic trachytes described by Liu Dong [16] and may have originated from partial melting of the thickened lower crust [16,52,53]. To summarize, ultrapotassic andesite with distinct mantle

characteristics is generated by partial melting of the enriched mantle. Potash trachyte and diorite are produced by the melting of the thickening lower crust. Ultrapotassic trachyte originates from the lower crust. However, these four types of volcanic rocks share some geochemical features, including enrichment in large ion lithophile elements and transition metals such Cr and Ni, high Th/Ta ratios, low Nd/La ratios, and low Rb/Ba ratios. They also exhibit similar trace element distribution patterns, indicating possible interaction among different magma source regions [54,55]. Therefore, we suggested that the four types of volcanic rocks in the Xiongba Formation are likely the result of magma activity response in different lithospheric layers under the same tectonic–magmatic setting [16].

5.2. Formation Mechanisms and Sources of Boron Enrichment in Volcanic Rocks

The B enrichment in magmas is a complex process that involves various sources and mechanisms. The original magma usually has a low boron content, which is mostly dispersed in rock-forming minerals such as plagioclase, K-feldspar, biotite, and quartz [56]. The average B abundance in the mantle is <0.1 ppm, while in the continental lithosphere and upper crust, it can reach 6.7–7.82 ppm and 15 ppm, respectively [56,57]. Thus, any B content higher than these values indicates an enrichment anomaly, which can result from the incorporation of B from external sources. Two main pathways have been proposed to explain the origin of B enrichment in magmas [57,58]. One is the underwater alteration of the oceanic crust, which releases boron into fluids that can infiltrate and modify the overlying mantle or crust. The other is the adsorption of boron by deep-sea sediments from seawater, which can later release boron during subduction and fluid-rock interaction. The subduction plates and sediments can host much higher boron concentrations than the mantle [59]. The content of trace elements in magmas can provide insights into their evolution and enrichment history. Although boron does not show significant changes during normal magmatic differentiation, it can reflect fluid enrichment when compared to relatively fluid-immobile elements such as La, Ce, Nb, Sm, Gd, Yb, and Zr [58–60]. In this study, the higher values of B/La, B/Ce, and B/Zr in the potassium trachyte andesite and potash trachyte indicate that boron was enriched in the magma [60]. The B/La and B/Ce ratios of the studied volcanic rocks ranged from 0.080 to 7.064 and from 0.035 to 3.371, respectively. The B/Zr ratios were 0.017 and 1.991, respectively, higher than the average B/Zr value of ocean island basalts (0.012) [60]. These high B/incompatible element ratios suggest that the magma experienced fluid enrichment from the dehydration of subducted oceanic crust [59,60]. The arc-like trace element features (e.g., Nb-Ta depletion relative to La and K) and high B concentrations in these rocks were inherited from the mantle source, which had been enriched by melt/fluid of the subducted sediments. Overall, B enrichment in magmas can result from the interaction of various components and processes, including subduction fluids, altered oceanic crust, and deep-sea sediments. The contents of REEs, such as Gd and Sm, in magmas can provide valuable information on their source and evolution. In this study, the Gd and Sm contents increase in the order of potash trachyte, ultrapotassium trachyte, ultrapotassic andesite, and potassium trachyte andesite (Figure 5d). This trend can be explained by the increasing degree of fractionation and differentiation in the magmas, which causes the enrichment of Gd and Sm [61]. Moreover, we found that the Gd and Sm contents of all studied samples show a positive correlation, suggesting these elements behave similarly during magmatic processes. The Gd and Sm contents of the potash trachyte are lower compared to the other samples, indicating the influence of fluid enrichment [50,51,54,55].

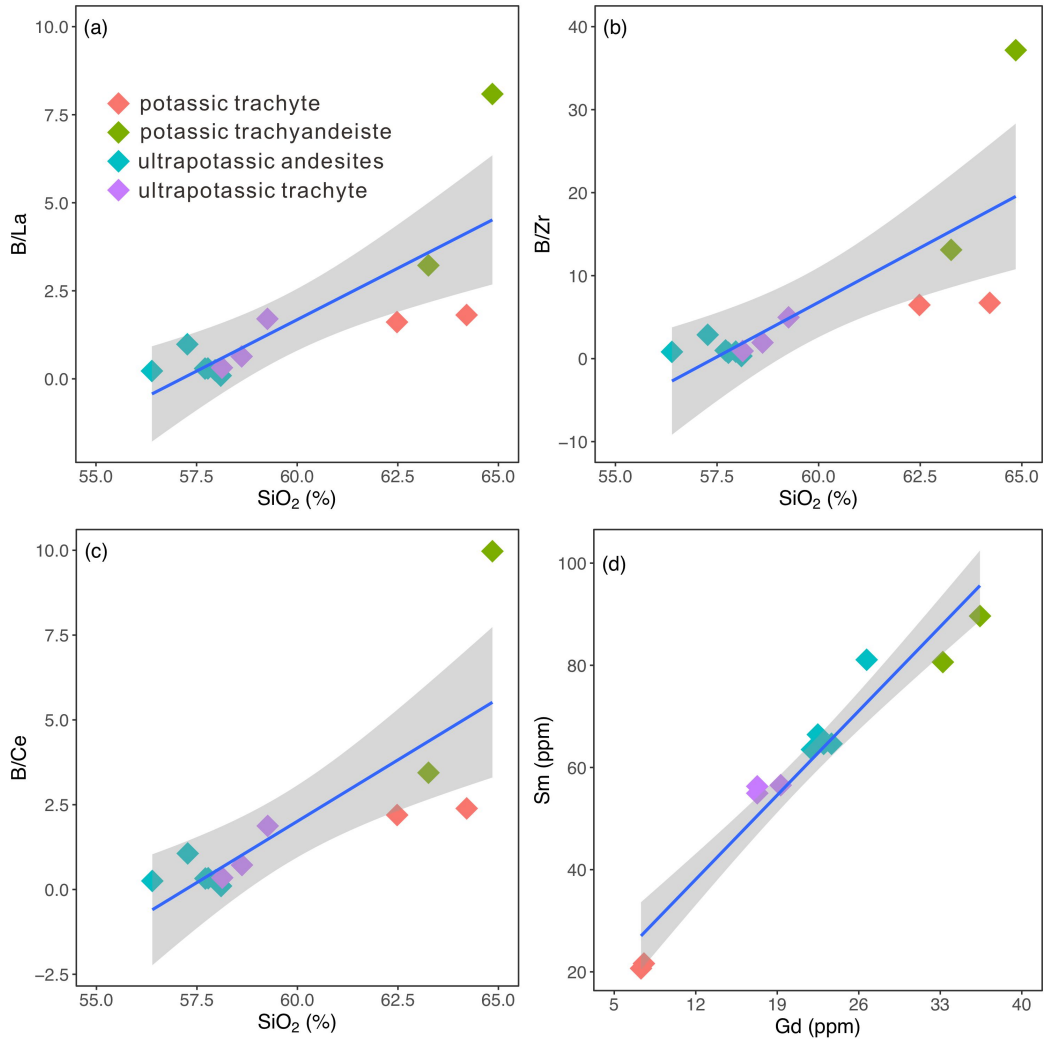

Figure 5. Plots of (**a**) B/La and SiO_2; (**b**) B/Zr and SiO_2; (**c**) B/Ce and SiO_2; (**d**) Sm and Gd.

The Pb/Ce ratio of marine sediments is often higher than that of oceanic basalts, indicating the involvement of subducted sediments in the formation of oceanic basalts [62]. The Pb/Ce ratio and Pb content in the studied volcanic rock are close to the area near the marine sediment, indicating that the magmas have assimilated marine sediment (Figure 6). This finding is further supported by the enrichment of Th in the samples, which is closely associated with the addition of sedimentary material to the mantle source region by subduction [63]. Moreover, the Ba/La and La/Sm ratios in arc volcanic rocks can be utilized not only to differentiate between island arc volcanic rocks and oceanic volcanic rocks but also to explain the involvement of a minor quantity of subducted deep-sea sediment in the magma source of arc volcanic rocks [62]. By examining the correlation analysis between the Ba/La and La/Sm ratios of the samples with the chondrite-normalized values (Figure 7), it is evident that the samples mainly fall within the boundary between marine sediments and island-arc basalts, indicating the characteristics of arc magmas and the possible participation of marine sediment in the magma activity. Furthermore, it is suggested that the magmas of potassic rocks may have assimilated biogenic sediment (Figure 8).

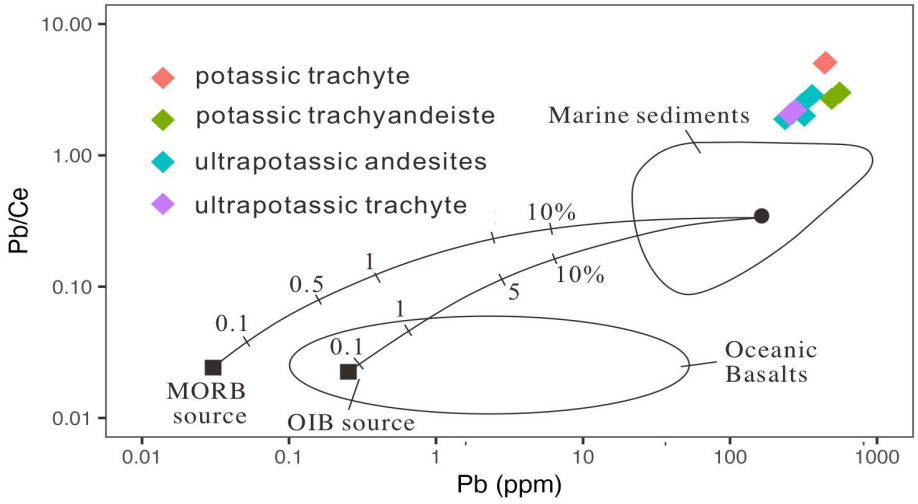

Figure 6. Pb/Ce ratios and Pb concentrations in studied volcanic rocks compared with oceanic basalts and marine sediments (modified from Othman et al., 1989 [62]). Two mixing curves are shown: one with average sediment and a calculated MORB source (depleted mantle) composition, the other with average sediment and an OIB source ("enriched mantle") composition. Numbers adjacent to ticks on mixing curves are the percent sediment in the mixture.

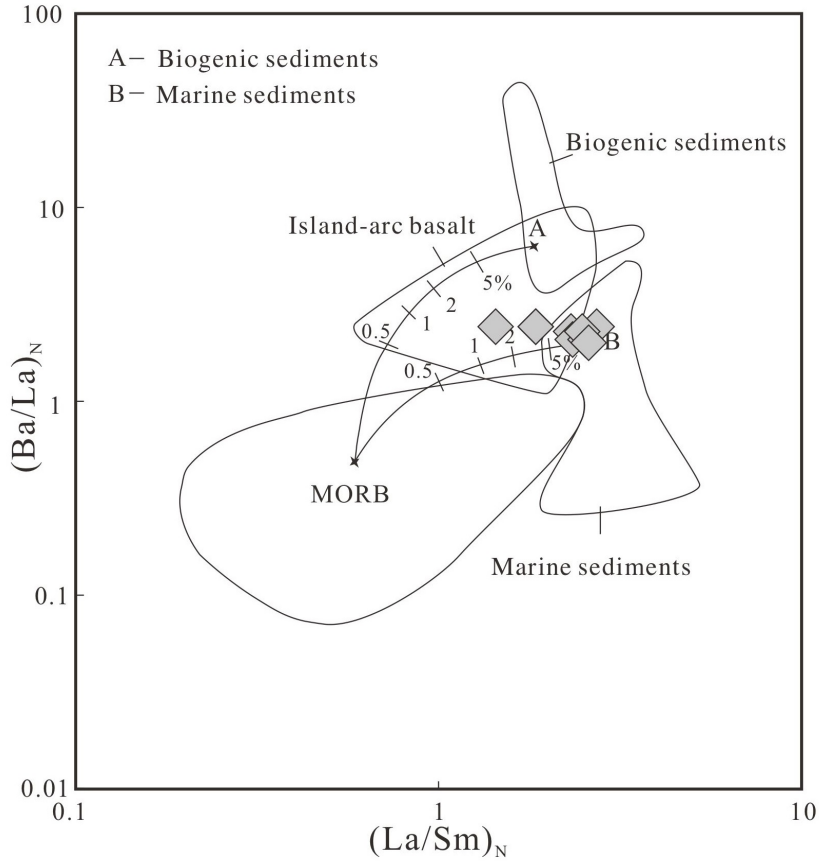

Figure 7. Chondrite-normalized Ba/La and La/Sm ratios in volcanic rocks in Xionba Basin. Two calculated mixing curves are shown. A is a high Ba/La Pacific biogenic sediment (DSDP 183-3-2 from Kay, 1984 [64]; Numbers adjacent to ticks on mixing curves are the percent sediment in the mixture. The MORB field is also shown.

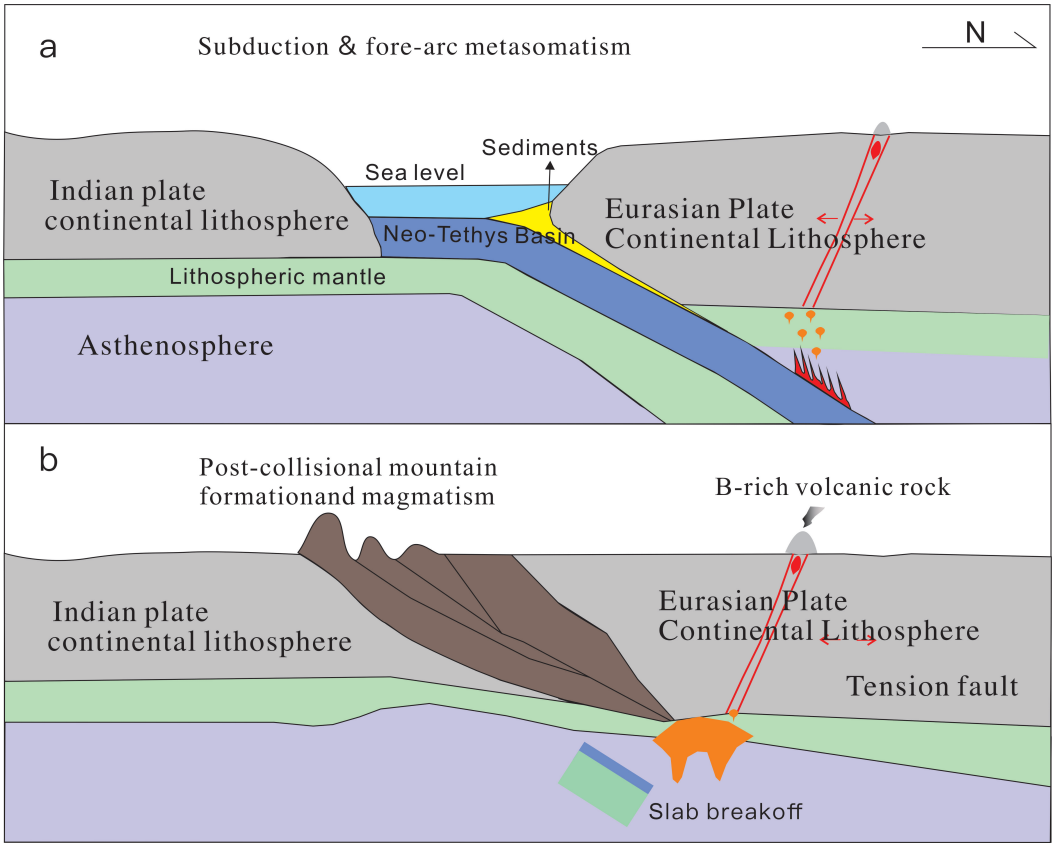

Figure 8. Diagram of the formation mechanism of B-rich volcanic rocks. A two-stage evolution model for the B enrichment in the subduction environment (**a**) and the melting of B-enriched source during the post-collisional setting (**b**).

5.3. Implication for the Origin of Lacustrine B-Rich Sediments in QTP

The subduction environment is a critical factor in the initial enrichment of boron in magma. The high mobility and incompatibility of boron allow for the altered oceanic crust and deep-sea sediments enriched in boron (and other related elements such as Li) to release boron during subduction metamorphism and dehydration processes [38,53,60,62]. As a result, large ion lithophile element end-member fluids are enriched with boron and carried into magma, leading to the enrichment of boron in the magma. The enriched fluid is released during magma eruption, resulting in the release of boron into volatiles [7]. The continuous subduction process leads to the gradual depletion of boron with the decomposition or reaction of the host rock containing boron. The B/Be and B/Nb ratios (see Table 1) decrease with increasing subduction depth, resulting in varying degrees of boron enrichment in magma at different depths. Although the volcanic rocks in the Xiongba Basin are in a post-collisional environment and have no direct relationship with the subduction zone, subduction can still cause boron enrichment in magma [65]. The Indian continental lithosphere underwent subduction at 25–16 Ma [38], and the crustal sediment carried down to the western Lhasa lithosphere under the ancient subduction zone resulted in boron enrichment in magma. The boron-enriched magma underwent degassing during the eruption, releasing boron into volatiles, which was then transported by the Xiong'er Fault to the Nie'er Lake and Zaching Caka drainage basins, becoming one of the primary sources of boron for boron minerals. Boron is also a potential "escape" element that is soluble in water solutions at medium to high temperatures (>100 °C) [65]. In the ancient subduction environments of the QTP, which is composed of multiple suture zones, shell-derived sediments may have been carried into the magma during the ancient subduction, leading to the enrichment of beneficial elements such as boron and lithium in volcanic rocks [29,38]. Boron's propensity for redistribution under the conditions of water solution

can cause the concentration of boron in rocks to change due to diagenesis, hydrothermal, or metamorphic processes [54,56]. This behavior is common in geothermal, hydrothermal, and mineralization environments. Therefore, the numerous boron- and lithium-rich hot springs developed in the Qinghai–Tibet Plateau are another significant source of boron for the current "special" salt lakes [66]. In summary, the subduction environment may play a crucial role in the initial B enrichment of the magma source. The boron-enriched magma undergoes degassing during the eruption, releasing boron into volatiles that can be transported by faults to different drainage basins, becoming one of the primary sources of boron for boron minerals. The solubility of boron in water solutions at medium to high temperatures can also cause the concentration of boron in rocks to change due to various geological processes, resulting in significant concentrations of boron in geothermal, hydrothermal, and mineralization environments.

6. Conclusions

This work investigated the volcanic rocks in Xiongba Basin, which are composed of four types of rocks classified: ultrapotassic andesites, ultrapotassic trachyte, ultrapotassic trachyte, and potassic trachyte. The arc-like trace element features (e.g., Nb-Ta depletion relative to La and K) and high B concentrations in these rocks were inherited from the mantle source, which had been enriched by melt/fluid of the subducted sediments. Subduction plays a crucial role in magma boron enrichment, and our results reveal that the volcanic rocks in the Xiongba Basin exhibit varying degrees of B enrichment, and the magma source was mainly influenced by subduction. The ultrapotassic andesite has the lowest boron content and ultrapotassic trachyte has the highest, as they formed at different subduction depths, suggesting that subduction is a critical factor in boron enrichment. Our study results indicate that the boron released during the degassing process of high-boron magma eruptions and post-eruption hydrothermal activities has been transported to the ancient lake basin. As a result, the presence of this type of volcanic rock can serve as an indicator of B and Li mineralization in the QTP. Our study provides insight into the geochemical characteristics of the volcanic rocks in the Xiongba Basin and their potential link to ancient subduction environments. Our findings reveal the crucial role of subduction in magma boron enrichment and the enrichment of beneficial elements such as B and Li in volcanic rocks. This work has significant implications for understanding the geological processes contributing to the formation of B and Li resources within salt lakes in the QTP.

Author Contributions: Conceptualization, W.C. and Y.L.; investigation, W.C.; writing—original draft preparation, W.C. and Y.L.; writing—review and editing, W.C., Y.L., X.L. and Y.Z.; funding acquisition, W.C. All authors have read and agreed to the published version of the manuscript.

Funding: This research is supported by the Second Tibetan Plateau Scientific Expedition and Research Program (2022QZKK0201), the Enterprise Collaboration Project (investigation on Comprehensive Metallogenic Conditions of Volcanic Sedimentary Boron Deposits in Xiongba Area, Geji County; Grant No. HE1304), and National Natural Science Foundation of China (Grant No. 42102115).

Data Availability Statement: Not applicable.

Acknowledgments: The authors wish to extend their heartfelt gratitude to the two anonymous reviewers and the academic editor for their invaluable insights and constructive feedback provided during the review process.

Conflicts of Interest: The authors declare no conflict of interest.

References

1. Stamatakis, M.G. A boron-bearing potassium feldspar in volcanic ash and tuffaceous rocks from Miocene lake deposits, Samos Island, Greece. *Am. Mineral.* **1989**, *74*, 230–235.
2. García-Veigas, J.; Helvacı, C. Mineralogy and sedimentology of the Miocene Göcenoluk borate deposit, Kırka district, western Anatolia, Turkey. *Sediment. Geol.* **2013**, *290*, 85–96. [CrossRef]
3. Borojević Šoštarić, S.; Brenko, T. The Miocene Western Balkan lithium-boron metallogenic zone. *Miner. Depos.* **2022**, *58*, 639–658. [CrossRef]

4. Dill, H.G.; Kaufhold, S.; Helvacı, C. The physical–chemical regime of argillaceous interseam sediments in the Emet borate district, Turkey: A transition from non-metallic volcano-sedimentary to metallic epithermal deposits. *J. Geochem. Explor.* **2015**, *156*, 44–60. [CrossRef]
5. Ortí, F.; Rosell, L.; García-Veigas, J.; Helvaci, C. Sulfate–Borate Association (Glauberite–Probertite) In the Emet Basin: Implications For Evaporite Sedimentology (Middle Miocene, Turkey). *J. Sediment. Res.* **2016**, *86*, 448–475. [CrossRef]
6. Song, L.R.; Yu, C.Q.; Li, G.H.; Feng, Y.Y.; He, J.J. Characteristics of gravity anomalies and prediction of volcanosedimentary boron deposit distribution in the Xiongba area, Tibet. *Appl. Geophys.* **2015**, *12*, 516–522. [CrossRef]
7. Floyd, P.; Helvaci, C.; Mittwede, S. Geochemical discrimination of volcanic rocks associated with borate deposits: An exploration tool? *J. Geochem. Explor.* **1998**, *60*, 185–205. [CrossRef]
8. Xia, L.; Li, X.; Ma, Z.; Xu, X.; Xia, Z. Cenozoic volcanism and tectonic evolution of the Tibetan plateau. *Gondwana Res.* **2011**, *19*, 850–866. [CrossRef]
9. Wang, Y.; Zhang, X.; Jiang, C.; Wei, H.; Wan, J. Tectonic controls on the late Miocene–Holocene volcanic eruptions of the Tengchong volcanic field along the southeastern margin of the Tibetan plateau. *J. Asian Earth Sci.* **2007**, *30*, 375–389. [CrossRef]
10. Che, D.; Zheng, M.; Zhao, Y.; Zhang, Z.; Ye, C.; Xing, E.; Zhang, X.; Li, M. High Degree of Differentiation and Enrichment of Li, Rb and Cs in Potassic-Ultrapotassic Volcanic Rocks: An Example from the Lhasa Block, Tibet. *Minerals* **2023**, *13*, 342. [CrossRef]
11. Su, W.; Cai, K.; He, Z.; Zhao, X.; Zhong, H.; Glorie, S.; de Grave, J. Late Oligocene to Pleistocene Thermo-Tectonic Evolution of the Karakoram Fault Zone: New Insights from Basement and Detrital Apatite Fission Track Thermochronology. *Available at SSRN 4402303* **2023**, *32*. [CrossRef]
12. Zheng, M.; Chen, W.; Qi, W. New Findings and Perspective Analysis of Prospecting for Volcanic Sedimentary Boron Deposits in the Tibetan Plateau. *Acta Geosci. Sin.* **2016**, *37*, 407–418. (In Chinese with English abstract)
13. Chang, C.f.; Pan, Y.S.; Sun, Y.Y. The tectonic evolution of Qinghai-Tibet Plateau: A review. In *Tectonic Evolution of the Tethyan Region*; Springer: Dordrecht, The Netherlands, 1989; pp. 415–476.
14. Yin, A.; Harrison, T.M. Geologic evolution of the Himalayan-Tibetan orogen. *Annu. Rev. Earth Planet. Sci.* **2000**, *28*, 211–280. [CrossRef]
15. Zhu, D.C.; Zhao, Z.D.; Niu, Y.; Dilek, Y.; Hou, Z.Q.; Mo, X.X. The origin and pre-Cenozoic evolution of the Tibetan Plateau. *Gondwana Res.* **2013**, *23*, 1429–1454. [CrossRef]
16. Liu, D.; Zhao, Z.; Zhu, D.; Wang, Q.; Sui, Q.; Liu, Y.; Hu, Z.; Mo, X. The petrogenesis of postcollisional potassic-ultrapotassic rocks in Xungba basin, western Lhasa terrane: Constraints from zircon U-Pb geochronology and geochemistry. *Acta Petrol. Sin.* **2011**, *27*, 2045–2059. (In Chinese with English abstract)
17. Yang, X.; Zhu, B.; White, P.D. Provenance of aeolian sediment in the Taklamakan Desert of western China, inferred from REE and major-elemental data. *Quat. Int.* **2007**, *175*, 71–85. [CrossRef]
18. Lin, Y.; Zheng, M.; Ye, C.; Power, I.M. Trace and rare earth element geochemistry of Holocene hydromagnesite from Dujiali Lake, central Qinghai–Tibetan Plateau, China. *Carbonates Evaporites* **2019**, *34*, 1265–1279. [CrossRef]
19. Taylor, S.R.; McLennan, S.M. *The Continental Crust: Its Composition and Evolution*; Blackwell Scientific: Oxford, UK, 1985.
20. Kamber, B.S.; Webb, G.E. The geochemistry of late Archaean microbial carbonate: Implications for ocean chemistry and continental erosion history. *Geochim. Cosmochim. Acta* **2001**, *65*, 2509–2525. [CrossRef]
21. Irvine, T.N.; Baragar, W. A guide to the chemical classification of the common volcanic rocks. *Can. J. Earth Sci.* **1971**, *8*, 523–548. [CrossRef]
22. BAS, M.L.; Maitre, R.L.; Streckeisen, A.; Zanettin, B.; IUGS Subcommission on the Systematics of Igneous Rocks. A chemical classification of volcanic rocks based on the total alkali-silica diagram. *J. Petrol.* **1986**, *27*, 745–750. [CrossRef]
23. Rickwood, P.C. Boundary lines within petrologic diagrams which use oxides of major and minor elements. *Lithos* **1989**, *22*, 247–263. [CrossRef]
24. Prelević, D.; Akal, C.; Foley, S.; Romer, R.; Stracke, A.; Van Den Bogaard, P. Ultrapotassic mafic rocks as geochemical proxies for post-collisional dynamics of orogenic lithospheric mantle: The case of southwestern Anatolia, Turkey. *J. Petrol.* **2012**, *53*, 1019–1055. [CrossRef]
25. Conticelli, S. The effect of crustal contamination on ultrapotassic magmas with lamproitic affinity: Mineralogical, geochemical and isotope data from the Torre Alfina lavas and xenoliths, Central Italy. *Chem. Geol.* **1998**, *149*, 51–81. [CrossRef]
26. Boynton, W.V. Cosmochemistry of the rare earth elements: Meteorite studies. In *Developments in Geochemistry*; Elsevier: Amsterdam, The Netherlands, 1984; Volume 2, pp. 63–114.
27. Sun, S.S.; McDonough, W.F. Chemical and isotopic systematics of oceanic basalts: Implications for mantle composition and processes. *Geol. Soc. Lond. Spec. Publ.* **1989**, *42*, 313–345. [CrossRef]
28. Wang, Q.; Zhu, D.C.; Zhao, Z.D.; Liu, S.A.; Chung, S.L.; Li, S.M.; Liu, D.; Dai, J.G.; Wang, L.Q.; Mo, X.X. Origin of the ca. 90 Ma magnesia-rich volcanic rocks in SE Nyima, central Tibet: Products of lithospheric delamination beneath the Lhasa-Qiangtang collision zone. *Lithos* **2014**, *198*, 24–37. [CrossRef]
29. Mo, X.; Zhao, Z.; Don, J.D.; Zhou, S.; Dong, G. Three types of collisional and post-collisional magmatism in the Lhasa block, Tibet and implications for India intra-continental subduction and mineralization: Evidence from Sr-Nd isotopes. *Acta Petrol. Sin.* **2006**, *22*, 795–803. (In Chinese with English abstract)

30. Dalslåen, B.H.; Gasser, D.; Grenne, T.; Augland, L.E.; Corfu, F. Ordovician shoshonitic to ultrapotassic volcanism in the central Norwegian Caledonides: The result of sediment subduction, mantle metasomatism and mantle partial melting. *Lithos* **2020**, *356*, 105372. [CrossRef]
31. Guo, Z.; Wilson, M.; Liu, J. Post-collisional adakites in south Tibet: Products of partial melting of subduction-modified lower crust. *Lithos* **2007**, *96*, 205–224. [CrossRef]
32. Mallik, A.; Nelson, J.; Dasgupta, R. Partial melting of fertile peridotite fluxed by hydrous rhyolitic melt at 2–3 GPa: Implications for mantle wedge hybridization by sediment melt and generation of ultrapotassic magmas in convergent margins. *Contrib. Mineral. Petrol.* **2015**, *169*, 48. [CrossRef]
33. Conticelli, S.; Avanzinelli, R.; Marchionni, S.; Tommasini, S.; Melluso, L. Sr-Nd-Pb isotopes from the Radicofani Volcano, Central Italy: constraints on heterogeneities in a veined mantle responsible for the shift from ultrapotassic shoshonite to basaltic andesite magmas in a post-collisional setting. *Mineral. Petrol.* **2011**, *103*, 123–148. [CrossRef]
34. Hofmann, A.W.; White, W.M. Mantle plumes from ancient oceanic crust. *Earth Planet. Sci. Lett.* **1982**, *57*, 421–436. [CrossRef]
35. Pearce, J.A.; Peate, D.W. Tectonic implications of the composition of volcanic arc magmas. *Annu. Rev. Earth Planet. Sci.* **1995**, *23*, 251–285. [CrossRef]
36. Sami, M.; Azer, M.; Abdel-Karim, A.A. Postcollisional Ferani Volcanics from North Arabian–Nubian Shield (South Sinai, Egypt): Petrogenesis and Implication for Ediacaran (607–593 Ma) Geodynamic Evolution. *J. Geol.* **2022**, *130*, 475–498. [CrossRef]
37. Rudnick, R.L.; Fountain, D.M. Nature and composition of the continental crust: A lower crustal perspective. *Rev. Geophys.* **1995**, *33*, 267–309. [CrossRef]
38. Zhao, Z.; Mo, X.; Luo, Z.; Zhou, S.; Dong, G.; Wang, L.; Zhang, F. Subduction of India beneath Tibet: Magmatism evidence. *Earth Sci. Front.* **2003**, *10*, 149–157. (In Chinese with English abstract)
39. Mitchell, R.H.; Bergman, S.C. *Petrology of Lamproites*; Springer Science & Business Media: Berlin/Heidelberg, Germany, 1991.
40. Castro, A.; Vogt, K.; Gerya, T. Generation of new continental crust by sublithospheric silicic-magma relamination in arcs: A test of Taylor's andesite model. *Gondwana Res.* **2013**, *23*, 1554–1566. [CrossRef]
41. Patiño Douce, A.E. Experimental generation of hybrid silicic melts by reaction of high-Al basalt with metamorphic rocks. *J. Geophys. Res. Solid Earth* **1995**, *100*, 15623–15639. [CrossRef]
42. Hu, W.; Tian, S.; Yang, Z.; Zhang, Z. Petrogenesis of Miocene Chajiasi potassic rocks in western Lhasa block, Tibetan Plateau: Constraints from lithogeochemistry, geochronology and Sr-Nd isotopes. *Miner. Depos.* **2012**, *31*, 813–830. (In Chinese with English abstract)
43. Garson, M.; Coats, J.; Rock, N.; Deans, T. Fenites, breccia dykes, albitites, and carbonatitic veins near the Great Glen Fault, Inverness, Scotland. *J. Geol. Soc.* **1984**, *141*, 711–732. [CrossRef]
44. Guo, Z.; Wilson, M.; Liu, J.; Mao, Q. Post-collisional, potassic and ultrapotassic magmatism of the northern Tibetan Plateau: Constraints on characteristics of the mantle source, geodynamic setting and uplift mechanisms. *J. Petrol.* **2006**, *47*, 1177–1220. [CrossRef]
45. Carminati, E.; Lustrino, M.; Doglioni, C. Geodynamic evolution of the central and western Mediterranean: Tectonics vs. igneous petrology constraints. *Tectonophysics* **2012**, *579*, 173–192. [CrossRef]
46. Wang, Q.; Xu, J.; Zhao, Z. The summary and comment on research on a new kind of igneous rock-adakite. *Adv. Earth Sci.* **2001**, *16*, 201–208. (In Chinese with English abstract)
47. Huang, W.L.; Wyllie, P. Phase relationships of S-type granite with H_2O to 35 kbar: Muscovite granite from Harney Peak, South Dakota. *J. Geophys. Res. Solid Earth* **1981**, *86*, 10515–10529. [CrossRef]
48. Cheng, Z.; Guo, Z. Post-collisional ultrapotassic rocks and mantle xenoliths in the Sailipu volcanic field of Lhasa terrane, south Tibet: Petrological and geochemical constraints on mantle source and geodynamic setting. *Gondwana Res.* **2017**, *46*, 17–42. [CrossRef]
49. Bonin, B.; Azzouni-Sekkal, A.; Bussy, F.; Ferrag, S. Alkali-calcic and alkaline post-orogenic (PO) granite magmatism: petrologic constraints and geodynamic settings. *Lithos* **1998**, *45*, 45–70. [CrossRef]
50. Samuel, M.; Moussa, H.; Azer, M. A-type volcanics in central eastern Sinai, Egypt. *J. Afr. Earth Sci.* **2007**, *47*, 203–226. [CrossRef]
51. Yücel, C.; Arslan, M.; Temizel, I.; Abdioğlu, E. Volcanic facies and mineral chemistry of Tertiary volcanics in the northern part of the Eastern Pontides, northeast Turkey: Implications for pre-eruptive crystallization conditions and magma chamber processes. *Mineral. Petrol.* **2014**, *108*, 439–467. [CrossRef]
52. Zhao, J.H.; Zhou, M.F. Neoproterozoic adakitic plutons in the northern margin of the Yangtze Block, China: Partial melting of a thickened lower crust and implications for secular crustal evolution. *Lithos* **2008**, *104*, 231–248. [CrossRef]
53. Vanderhaeghe, O.; Teyssier, C. Partial melting and flow of orogens. *Tectonophysics* **2001**, *342*, 451–472. [CrossRef]
54. Leeman, W.; Hawkesworth, C. Open magma systems: Trace element and isotopic constraints. *J. Geophys. Res. Solid Earth* **1986**, *91*, 5901–5912. [CrossRef]
55. McMillan, N.J.; Dickin, A.P.; Haag, D. Evolution of magma source regions in the Rio Grande rift, southern New Mexico. *Geol. Soc. Am. Bull.* **2000**, *112*, 1582–1593. [CrossRef]
56. Leeman, W.P.; Carr, M.J.; Morris, J.D. Boron geochemistry of the Central American volcanic arc: Constraints on the genesis of subduction-related magmas. *Geochim. Cosmochim. Acta* **1994**, *58*, 149–168. [CrossRef]
57. Marschall, H.R. Boron isotopes in the ocean floor realm and the mantle. *Boron Isotopes: The Fifth Element*; Springer: Berlin/Heidelberg, Germany, 2018; pp. 189–215.

58. Palmer, M.R.; Swihart, G.H. Boron isotope geochemistry: An overview. In *Boron*; De Gruyter: Berlin, Germany, 2018; pp. 709–744.
59. Tenthorey, E.; Hermann, J. Composition of fluids during serpentinite breakdown in subduction zones: Evidence for limited boron mobility. *Geology* **2004**, *32*, 865–868. [CrossRef]
60. Leeman, W.P. Implications for Subduction Processes. *Subduction Top Bottom* **1996**, *96*, 269.
61. Humphris, S.E. The mobility of the rare earth elements in the crust. In *Developments in Geochemistry*; Elsevier: Amsterdam, The Netherlands, 1984; Volume 2, pp. 317–342.
62. Othman, D.B.; White, W.M.; Patchett, J. The geochemistry of marine sediments, island arc magma genesis, and crust-mantle recycling. *Earth Planet. Sci. Lett.* **1989**, *94*, 1–21. [CrossRef]
63. Johnson, M.C.; Plank, T. Dehydration and melting experiments constrain the fate of subducted sediments. *Geochem. Geophys. Geosyst.* **2000**, *1*. [CrossRef]
64. Kay, R. Elemental abundances relevant to identification of magma sources. *Philos. Trans. R. Soc. Lond. Ser. A Math. Phys. Sci.* **1984**, *310*, 535–547.
65. Gméling, K.; Németh, K.; Martin, U.; Eby, N.; Varga, Z. Boron concentrations of volcanic fields in different geotectonic settings. *J. Volcanol. Geotherm. Res.* **2007**, *159*, 70–84. [CrossRef]
66. Zhang, W.; Tan, H.; Xu, W.; Huang, J. Boron source and evolution of the Zabuye salt lake, Tibet: Indication from boron geochemistry and isotope. *Appl. Geochem.* **2023**, *148*, 105516. [CrossRef]

Disclaimer/Publisher's Note: The statements, opinions and data contained in all publications are solely those of the individual author(s) and contributor(s) and not of MDPI and/or the editor(s). MDPI and/or the editor(s) disclaim responsibility for any injury to people or property resulting from any ideas, methods, instructions or products referred to in the content.